Charging Pad as the Transformer: Integration of On-board Charger, Auxiliary Power Module and Wireless Charger for Electric Vehicles

Liyan Zhu
Department of Electrical Engineering and Computer Science
University of Tennessee
Knoxville, TN, USA
liyan@utk.edu

Ziwei Liang
Department of Electrical Engineering and Computer Science
University of Tennessee
Knoxville, TN, USA
zliang7@utk.edu

Yue Sun
Department of Electrical Engineering and Computer Science
University of Tennessee
Knoxville, TN, USA
ysun79@utk.edu

Jie Li
Department of Electrical Engineering and Computer Science
University of Tennessee
Knoxville, TN, USA
jli94utk@gmail.com

Ruiyang qin
Department of Electrical Engineering and Computer Science
University of Tennessee
Knoxville, TN, USA
ruiyangq@gmail.com

Arka Basu
Department of Electrical Engineering and Computer Science
University of Tennessee
Knoxville, TN, USA
abasu1@vols.utk.edu

Daniel Costinett
Department of Electrical Engineering and Computer Science
University of Tennessee
Knoxville, TN, USA
dcostine@utk.edu

Hua Bai
Department of Electrical Engineering and Computer Science
University of Tennessee
Knoxville, TN, USA
hbai2@utk.edu

2023 IEEE Energy Conversion Congress and Exposition (ECCE) | 979-8-3503-1644-5/23/$31.00 ©2023 IEEE | DOI: 10.1109/ECCE53617.2023.10362363

***Abstract*— Integrated chargers have gained an increasing interest in the electric vehicle (EV) industry. Existing solutions such as the integrated onboard charger (OBC) and auxiliary power module (APM) save the cost and the size, however, it only provides limited functions and hard to be integrated with the future wireless power transfer (WPT) technology. This paper proposed a multi-function magnetic coupler-based integrated charger that provides bidirectional OBC, WPT charging, and APM functions in a single system. In addition to the multi-port converter topology, a multi-winding WPT charging pad is repurposed serving as the main transformer in the OBC and APM modes as well. The paper briefs the system topology, explains various charging modes, and details the magnetic coupler design. Furthermore, a prototype was constructed and successfully delivered 6.6kW in OBC mode, 3.3kW in V2L mode, 6.6kW in WPT mode, and 800W in APM mode, which validates the proposed design.**

Keywords—Onboard charger, Auxiliary power module, wireless charging, electric vehicles, wide-bandgap devices

I. INTRODUCTION

Promoting the widespread adoption of electric vehicles (EVs) relies significantly on the advancement of charging systems, which play a crucial role in mitigating mileage anxiety and enhancing user satisfaction [1]. While conductive charging, such as OBCs, offers cost-effectiveness and speed, it comes with the drawback of heavy charging cables and potential inconvenience during the charging process. In response to the need for improved charging convenience, industries are actively exploring solutions based on Wireless Power Transfer (WPT) [2],[3]. Although WPT-based charging presents a hassle-free option, it tends to be expensive and may have limitations in charging power [4],[5]. Some EVs are now equipped with both OBC and WPT chargers, affording users the choice of charging speed or experience. However, this dual-charging system could lead to increased bulkiness and higher costs. Moreover, the integration of the APM for charging the 12V battery further contributes to the overall cost and size of the charging system.

In the conventional approach, the design, manufacturing, and installation of OBC, WPT, and APM have been carried out as separate entities. This has necessitated the utilization of a complex cooling system, intricate unit geometry, and consequently led to higher expenses and larger dimensions. While mechanical integration has been employed to enhance the charging unit's compactness, it merely results in cost savings concerning the enclosure and cooling system. For the upcoming generation of integrated charging systems, there is a strong inclination towards embracing high-level topological and magnetic integration, as it holds greater appeal and promise.

An OBC+APM integrated charger has drawn increasing interest due to its simplicity and cost reduction. To achieve the integration of OBC and APM, a dual transformer configuration is employed, effectively combining the rectifier functions[6]. This integration is further enhanced through the utilization of a three-port transformer, which facilitates the creation of both a voltage-fed triple-active bridge (VFTAB) [7] and a current-fed triple-active bridge (CFTAB)[8]. The topologies based on the

three-port transformer as abstracted in Fig. 1, with less active and passive components to ensure the cost reduction.

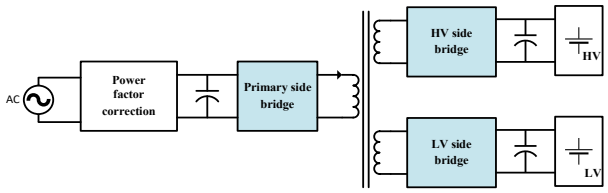

Fig. 1 Typical structure of integrated OBC+APM

Simultaneously, researchers have explored the integration of OBC and WPT using a shared full bridge, as detailed in [9]. However, this approach requires additional magnetic components, making it less optimal in terms of simplicity. Subsequent efforts to achieve further integration by combining shared full bridges with magnetic components have been proposed in [10]. Nevertheless, this approach poses challenges due to the complexity of the magnetic coupler, which hinders seamless integration with other functions, such as APM. A more effective integration method of WPT charging to the wired charging system with a simple structure and low cost is still missing.

To integrate the WPT, OBC, and APM, this paper proposed a novel solution that integrates magnetic components. Similar to Fig. 1, one more magnetic coupling is introduced to enable the WPT charging function, as shown in Fig. 2. Compared with the concept of integrated OBC+APM, a new loose coupling between the WPT transmitter pad and the onboard part is established, while the onboard parts still keep the tight coupling between the power factor controller (PFC), high-voltage (HV) and low-voltage (LV) ports.

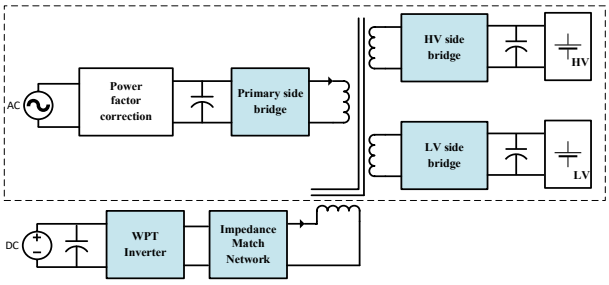

Fig. 2 proposed integration concept with a multi-purpose magnetic coupler

In this paper, a pioneering endeavor is made to integrate OBC, WPT, and APM using a straightforward multi-port topology. This innovative approach maximizes component sharing, effectively eliminating redundant power stages. The idea of utilizing the multi-winding receiver pad as the transformer further eliminates the conventional transformer and exhibits a reduction of cost and size. The paper is structured in the following manner: Section II provides an introduction to the system design and outlines the basic operation principles for different modes. Section III presents the design method for the proposed magnetic coupler. Simulation and experimental results are presented in Section IV. Finally, Section V contains the conclusion of the study.

II. Proposed Integration Solution

The proposed solution mainly includes the multi-port topology and multi-purpose magnetic coupler. The magnetic coupler serves as either the main transformer or the receiver pad for the WPT mode. The detailed topology and the operational principles of each charging mode are discussed in the section.

A. Topology

The proposed integrated EV charger is shown in

Fig. 3, including two major subsystems, i.e., the onboard part and off-board part. The on-board part is installed on the EV, and it can work alone as an integrated OBC+APM, or work as the receiver side in WPT charging mode.

As of the onboard unit, W1-W4 represent the windings that constitute a versatile magnetic coupler. Among these, W2 is shared and fulfills multiple functions, acting as the secondary winding of the OBC, the receiver coil for WPT, and the primary winding of the APM. In the OBC mode, the system is designed to accommodate a 3-Φ 480 Vac AC input and support a DC bus voltage of up to 800 V. To achieve this, a multi-level topology utilizing 650V GaN devices is adopted. Specifically, Qa1-Qa6 together create a three-level (3-L) active-neutral-point-clamp (ANPC) phase leg, while the 3-Φ legs constitute the complete AC-DC stage. Additionally, P1-P4, S11-S14, and S31-S34 are employed in a triple-active-bridge (TAB) converter configuration, featuring a voltage-fed (VF) port on HV side and a current-fed (CF) port on the LV side.

A three-level boost converter is in series with the HV battery as an interface. C_b is the dc blocking cap, L_{o1} is the inductor of the boost converter for OBC and WPT, and L_{o2}~L_{o3} is the coupled filter inductor for APM. This boost converter plays different roles in different charging modes. For example, in WPT mode, the boost converter matches the output voltage from the rectifier and the HV battery and controls the charging power. In APM mode, the converter works as a buck converter to minimize the voltage applied to the CFDAB stage.

The off-board unit mainly consists of an inverter, an impedance match network (IMN), and a transmitter pad. S_{41}-S_{44} forms the WPT inverter. The inductor-capacitor-capacitor-series (LCC-S) compensation topology consisting of L_{r1}, C_{r1}, $C_{r2,}$ and C_{r3} is adopted for IMN to deliver a constant output voltage on the secondary side.

B. Bidirectional OBC Mode

During operation in the OBC mode, the system involves three stages: PFC, Primary (Pri), and HV ports of the TAB converter, along with the boost converter. In this mode, the DC-DC stage operates at a significantly higher frequency than the resonant frequency in the WPT mode. Consequently, the impedance of Cb and C3 can be disregarded, leading the

converter to function as a dual-active-bridge (DAB) converter. The transferred power is

$$P_o \approx \frac{nV_1V_2}{2f_{OBC}L_{sOBC}}\phi(1-\phi) = \frac{nV_{dc}V_{hv}}{4f_{sOBC}L_{sOBC}}\phi_{hv}(1-\phi_{hv}) \quad (1)$$

Here, variables used in the context is define as:

- n represents the turn ratio of W1 and W2.

- Vdc denotes the DC bus voltage.

- Vhv signifies the output voltage of the dual-active-bridge (DAB) converter.

- f_{OBC} corresponds to the switching frequency in the OBC mode.

- Ls_{OBC} represents the equivalent leakage inductance referred to the primary side.

- ϕ_hv denotes the phase shift between P1 and S11.

The utilization of LCC-S compensation ensures a constant voltage gain regardless of the load conditions. To prevent any adverse effects on the primary side, relay K_{pri} will be kept open during this mode. The WPT inverter will operate under an open-loop control strategy. At the receiver side, a zero-current-detection (ZCD) based synchronized rectifier control is employed to enhance overall system efficiency. This approach enables efficient power transfer while maintaining synchronization between the transmitter and receiver components.

D. APM Mode

During the APM mode, the LV battery will be charged by the HV battery using the TAB converter with a voltage-fed HV port and a current-fed LV port, abbreviated as VF-CFDAB. This configuration is specifically chosen to circumvent the need for a high transformer turn ratio, resulting in lower current stress

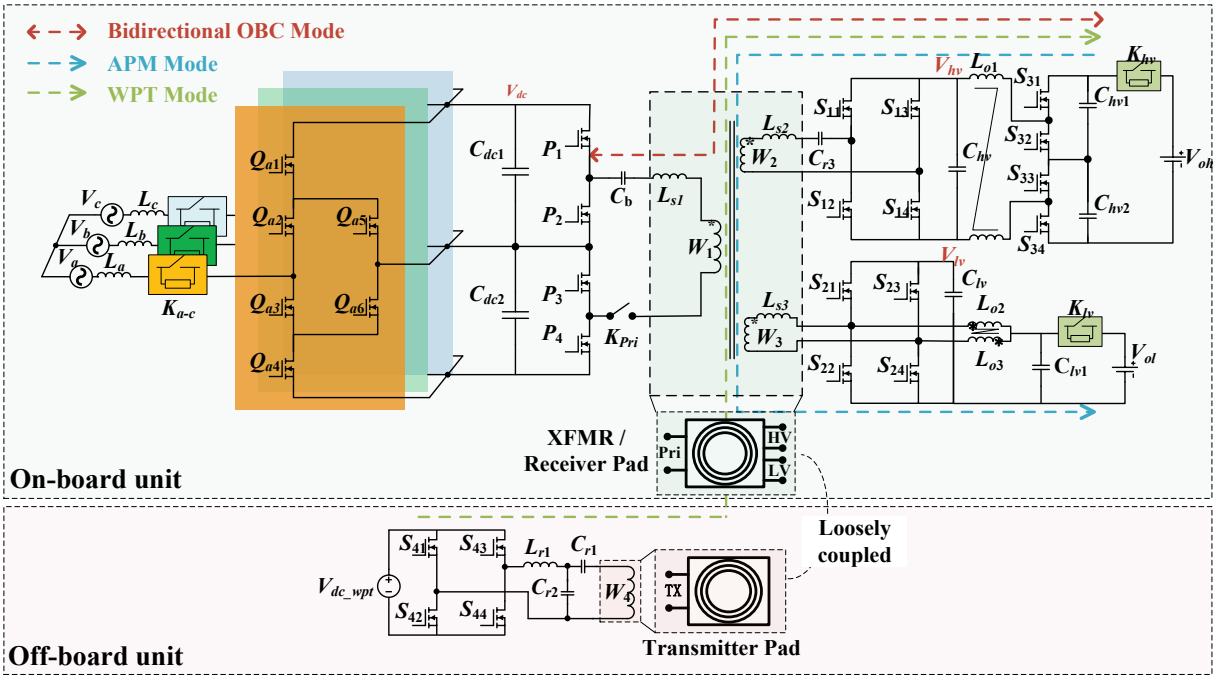

Fig. 3 Proposed topology of the fully integrated EV charger

C. WPT Mode

During the WPT mode, the operating frequency is deliberately reduced to facilitate the system's transition into the resonance mode, i.e.,

$$2\pi f_{WPT} = \frac{1}{\sqrt{L_2C_{r3}}} = \frac{1}{\sqrt{L_{r1}C_{r2}}} = \frac{1}{\sqrt{L_4\frac{C_{r1}C_{r2}}{C_{r1}+C_{r2}}}} \quad (2)$$

Ignoring the coil resistance, the voltage gain is simplified as

$$G_v \approx \frac{M_{24}}{L_{r1}} \quad (3)$$

on the LV side switches. A simplified triple phase shift (TPS) control is implemented. The boundary that separates mode 1 and mode 2 is expressed as follows:

$$D_{hv} \geq D_{lv} + \phi_{lv} \quad (4)$$

where D_{hv} and D_{lv} are the duty cycle of the HV and LV side. ϕ_{lv} is the phase shift between the HV and the LV sides. When $D_{hv} \geq D_{lv} + \phi_{lv}$, the output power of is

$$P_{op1} = \frac{n_2\phi_{lv}T_sV_{hv}V_{ol}}{n_3L_{sAPM}} \quad (5)$$

where n_2 *and* n_3 are the turns number of W_2 and W_3, V_{ol} is the LV battery voltage, and equivalent leakage inductance from the HV to LV ports is referred as L_{sAPM} .

III. Magnetic Coupler Design

The novel magnetic coupler is the key enabler of the work. The cross-sectional view of the transmitter and receiver pads and the explosive view of the receiver pad are shown in Fig. 4. The receiver pad consists of one flat ferrite plate on the top, and a plastic frame at the bottom. Three windings W1, W2, and W3 are sandwiched in between. Functioning as a highly coupled three-winding transformer, the windings are arranged on the same surface and attached as close to the ferrites as possible. The turns of each winding are determined by the target turn ratio, and the distance between coils is selected to obtain a preferred leakage inductance.

In addition to the receiver pad, one transmitter pad with a similar structure is designed, with only one coil needed, and it is loosely coupled to the receiver pad due to the charging distance requirement.

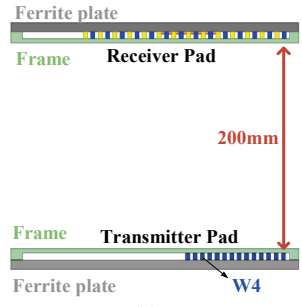

Fig. 4 Charging pads structure: (a) sectional view of two pads, (b) explosive view of the receiver pad.

In this study, a comprehensive design method is presented and illustrated in Fig. 7. The turn ratio is carefully set to 14:14:1 to ensure compatibility with the nominal voltages of both the HV and LV batteries, as specified in Table. I. To achieve this configuration, W1, W2, and W3 are arranged in a stacked manner within the receiver pad frame.

Specifically, W1 and W2 consist of 14-turn spiral coils, while W3 comprises a 1-turn spiral coil with 8 conductors in parallel. The use of parallel conductors in W3 allows for the avoidance of thick wires, thereby enhancing the coupling between the HV and LV windings. This paralleling design is crucial in optimizing the system's performance and efficiency during power transfer. One particular attention needed in the receiver pad design is the leakage inductance control between the Pri, HV and the LV coils, since the leakage inductances limit the maximal attainable power in each corresponding charging mode, as suggested in (1) and (5). The leakage between Pri and HV coils is controlled by the arrangement method of coils, and the inner and outer diameter of coils, while the HV to LV leakage is controlled by the relative position of the LV coils to other coils.

As illustrated in Fig. 5, two methods of winding arrangement are investigated to evaluate the impacts on the leakage inductance. The vertical arrange method delivers a primary side leakage of 3.7uH, an HV side leakage of 4uH, and an LV side leakage of 0.25uH. While the Pri and HV sides are well controlled by the winding inner and outer diameters, the LV leakage is too large to be used. To shrink the LV leakage inductance, the horizontal LV as shown in Fig. 5(b) is used. It enhanced the coupling between the LV and HV, thus effectively reducing the leakage inductance at the LV side to <0.2uH, which is close to the design target. The leakage can be then further tuned by the winding diameters, as shown in Fig. 6.

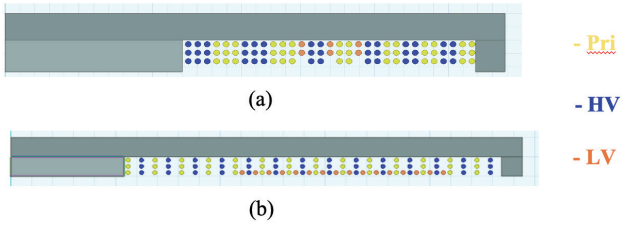

Fig. 5 Winding arrangement: (a) vertical LV (b) horizontal LV

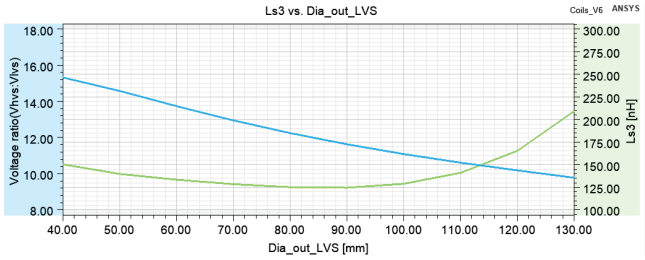

Fig. 6 Voltage ratio and LV leakage inductance vs the winding outer diameter

The transmitter pad is constructed with a single 14-turn spiral coil. To improve the coupling efficiency, each pad, including the transmitter and receiver pads, is equipped with 25 individual Mn-Zn ferrite cores, each measuring 50×50×4 mm in size. Both the transmitter and receiver pads have an outer diameter of 500mm. This configuration is specifically designed to facilitate a wireless power transfer (WPT) of 6.6kW with a charging distance of 200mm. The chosen dimensions and core arrangement are essential in achieving an optimal power transfer performance while ensuring efficient energy transmission over the specified distance.

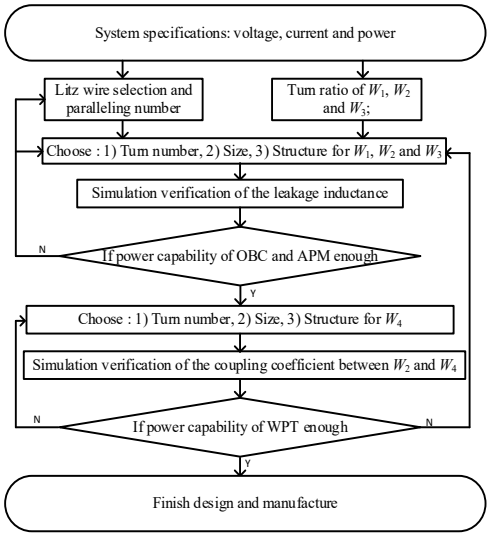

Fig. 7 Flowchart of the magnetic coupler design

Table. I SYSTEM SPECIFICATIONS

Parameter	f_{OBC}	f_{APM}	f_{WPT}	L_{r1}	C_{r1}	C_{r2}
Value	240 kHz	100 kHz	42.5 kHz	63.3μH	85 nF	250 nF
Parameter	C_{r3}	V_{ac}	V_{dcbus}	V_{dc_WPT}	V_{bat_HV}	V_{bat_LV}
Value	176 nF	380 V	650 V	400 V	350 V	12 V

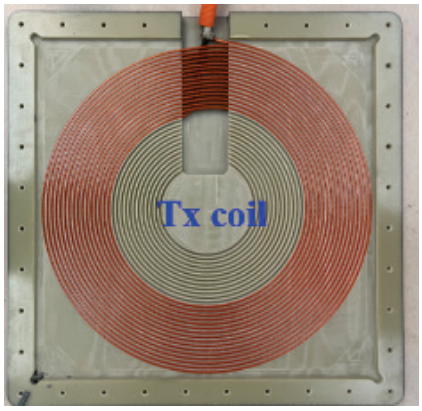

(a)

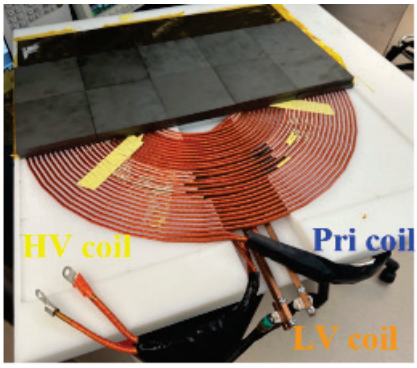

(b)

Fig. 8 Manufactured pads: (a) Transmitter pad, (b) Receiver pad.

The measured parameters of the magnetic coupler are presented in Table II. The table includes the following parameters:

- L1, L2, L3, and L4 represent the self-inductances of the respective coils.

- Ls1, Ls2, and Ls3 are the calculated leakage inductances.

- Lm denotes the magnetization inductance.

- k12, k23, and k24 are the coupling coefficients between the coils.

To calculate the measured equivalent leakage inductance for the OBC and APM modes, the impedance of Cr3 needs to be considered.

$$L_{sOBC}=L_{s1}+L_{s2}-\frac{1}{\omega_{OBC}^2 C_{r3}}=4.31\mu H$$
$$L_{sAPM}=L_{s2}+\left(\frac{n_2}{n_3}\right)^2 L_{s3}-\frac{1}{\omega_{APM}^2 C_{r3}}=47.9\mu H \quad (6)$$

These leakage inductances limit the max power in OBC and APM modes, which based on (1) and (5) are13 kW for OBC and 1.5 kW for APM.

Table. II MAGNETIC COUPLER PARAMETERS

Parameter	L_1	L_2	L_3	L_4	L_{s1}
Value	90.3 μH	86 μH	1.47 μH	212 μH	5.23 μH
Parameter	L_{s2}	L_{s3}	k_{12}	k_{23}	k_{24}
Value	1.58 μH	0.31 μH	0.975	0.66	0.133

IV. SIMULATION AND EXPERIMENTAL VALIDATION

A prototype, which includes both the on-board charger/APM and off-board WPT inverter, has been successfully constructed, as depicted in Fig. 9. Simulated magnetic field results for the core in OBC, APM, and WPT modes are illustrated in Fig. 10. The maximum magnetic flux densities recorded are 0.08T, 0.012T, and 0.013T for 6.6kW WPT, 6.6kW OBC, and 1.5kW APM, respectively.

The simulations have effectively verified that, apart from serving the WPT function, the core plates in the proposed magnetic coupler also satisfy the requirements for OBC and APM modes. This achievement is significant as it negates the need for additional cores or separate transformers, making the design more compact and efficient. The integrated magnetic coupler has proven its versatility and practicality in the different charging modes, validating its potential for real-world applications.

In addition, the LV side coils use multi-turn litz wires in parallel to handle the high current. The current distribution in each turn is simulated as Fig. 11. The results show a relatively high current in the outer and inner turn, but the peak current is still below the safe current rating of the wire, and all the other turns show a pretty evenly distributed current.

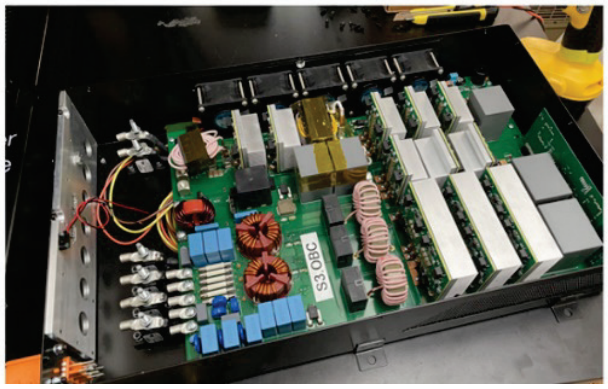

(a)

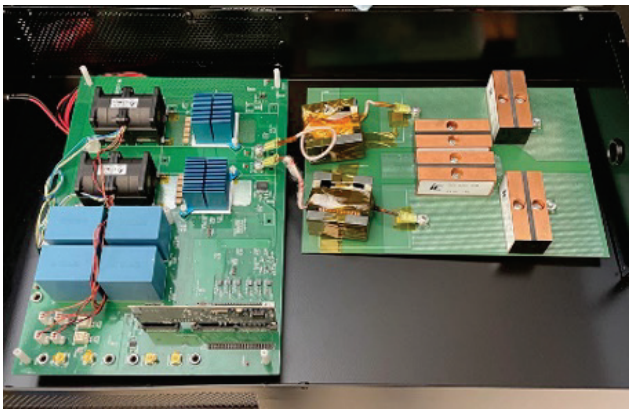

(b)

Fig. 9 Experimental prototype: (a) On-board charger, (b) Off-board WPT inverter and LCC compensation tank

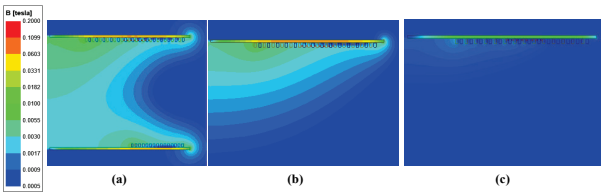

Fig. 10 Simulated flux density distribution: (a) WPT, (b) OBC, (c) APM

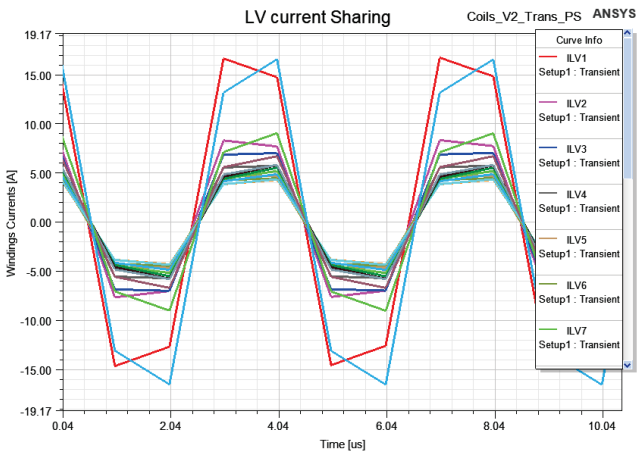

Fig. 11 Current distribution between turns of LV windings

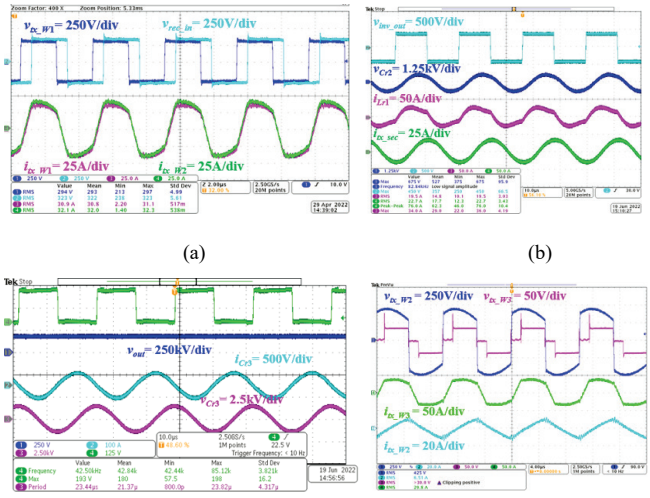

Fig. 12 Key waveforms: (a) OBC; (b) WPT inverter; (c) WPT secondary sync rectifier; (d) APM mode

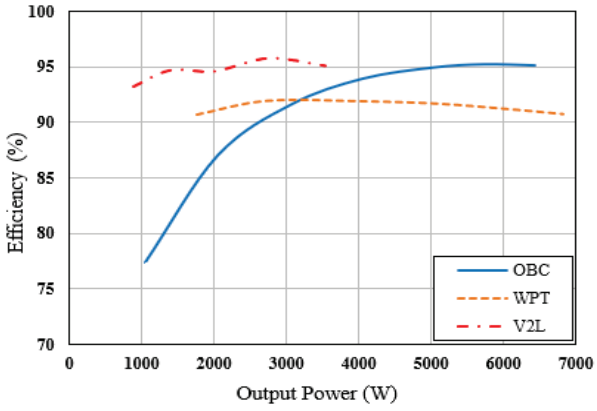

(a)

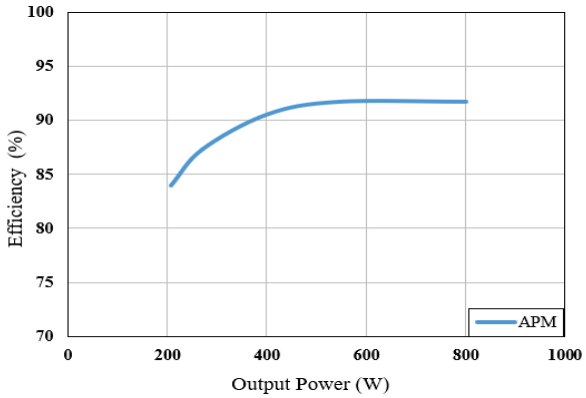

(b)

Fig. 13 Efficiency of different modes: (a) OBC, WPT and V2L, (b) APM.

Preliminary tests have been performed, encompassing various modes, such as 6.6 kW OBC, 6.6 kW WPT, 3.7 kW V2L, and 800 W APM. To emulate the battery during OBC, WPT, and APM tests, a battery emulator is utilized. For the V2L mode, a fixed resistive load of 22Ω is employed. Fig. 12 illustrates the key waveforms obtained during these tests, offering valuable insights into the system's performance. Additionally, the measured efficiency curves are displayed in Fig. 13, shedding light on the efficiency of the different modes. Notably, the boost stage plays a crucial role in the V2L mode, facilitating voltage matching of the DAB stage, which results in higher efficiency under light load conditions as compared to the OBC mode. These results indicate the successful operation and performance of the proposed integrated charging system in various modes, offering promising prospects for practical applications.

V. Conclusion

In order to provide WPT, OBC (with V2L mode), and APM capabilities, a unique multi-purpose magnetic coupler-based integrated charger was developed in this article. One single pad may serve as the transformer for the OBC and APM modes as well as the receiving pad for the WPT mode by having numerous windings built into the magnetic coupler. A multi-port converter is also included in the suggested design to connect the PFC, the HV battery, and the LV battery, saving two active bridges over the discrete version. The success of the suggested method was confirmed by the experimental findings, which examined the charging performance of each charging mode.

References

[1] H. K. Bai *et al.*, "Charging Electric Vehicle Batteries: Wired and Wireless Power Transfer: Exploring EV charging technologies," *IEEE Power Electron. Mag.*, vol. 9, no. 2, pp. 14–29, Jun. 2022, doi: 10.1109/MPEL.2022.3173543.

[2] X. Yu, J. Feng, and Q. Li, "A Planar Omnidirectional Wireless Power Transfer Platform for Portable Devices," in *2023 IEEE Applied Power Electronics Conference and Exposition (APEC)*, Mar. 2023, pp. 1654–1661. doi: 10.1109/APEC43580.2023.10131566.

[3] S. Li, Z. Liu, H. Zhao, L. Zhu, C. Shuai, and Z. Chen, "Wireless Power Transfer by Electric Field Resonance and Its Application in Dynamic Charging," *IEEE Trans. Ind. Electron.*, vol. 63, no. 10, pp. 6602–6612, Oct. 2016, doi: 10.1109/TIE.2016.2577625.

[4] X. Wang, J. Xu, H. Ma, and P. Yang, "A High Efficiency LCC-S Compensated WPT System With Dual Decoupled Receive Coils and Cascaded PWM Regulator," *IEEE Trans. Circuits Syst. II Express Briefs*, vol. 67, no. 12, pp. 3142–3146, Dec. 2020, doi: 10.1109/TCSII.2020.2973770.

[5] Y. Zhang *et al.*, "Misalignment-Tolerant Dual-Transmitter Electric Vehicle Wireless Charging System With Reconfigurable Topologies," *IEEE Trans. Power Electron.*, vol. 37, no. 8, pp. 8816–8819, Aug. 2022, doi: 10.1109/TPEL.2022.3160868.

[6] G. Yu and S. Choi, "An Effective Integration of APM and OBC With Simultaneous Operation and Entire ZVS Range for Electric Vehicle," *IEEE Trans. Power Electron.*, vol. 36, no. 9, pp. 10343–10354, Sep. 2021, doi: 10.1109/TPEL.2021.3063931.

[7] I. Kougioulis, P. Wheeler, and M. R. Ahmed, "An Integrated On-Board Charger and Auxiliary Power Module for Electric Vehicles," in *2022 IEEE Applied Power Electronics Conference and Exposition (APEC)*, Mar. 2022, pp. 1162–1169. doi: 10.1109/APEC43599.2022.9773777.

[8] L. Zhu, H. Bai, A. Brown, and L. Keuck, "A Current-fed Three-port DC/DC Converter for Integration of On-board Charger and Auxiliary Power Module in Electric Vehicles," in *2021 IEEE Applied Power Electronics Conference and Exposition (APEC)*, Jun. 2021, pp. 577–582. doi: 10.1109/APEC42165.2021.9487263.

[9] M. Elshaer, C. Bell, A. Hamid, and J. Wang, "DC–DC Topology for Interfacing a Wireless Power Transfer System to an On-Board Conductive Charger for Plug-In Electric Vehicles," *IEEE Trans. Ind. Appl.*, vol. 57, no. 6, pp. 5552–5561, Nov. 2021, doi: 10.1109/TIA.2021.3103700.

[10] Y. Zhang *et al.*, "Integration of Onboard Charger and Wireless Charging System For Electric Vehicles With Shared Coupler, Compensation, and Rectifier," *IEEE Trans. Ind. Electron.*, vol. 70, no. 7, pp. 7511–7514, Jul. 2023, doi: 10.1109/TIE.2022.3204857.